APPLICATION OF THE NIST 18 TERM ERROR MODEL TO CYLINDRICAL NEAR-FIELD ANTENNA MEASUREMENTS

Allen C. Newell*, David Lee**

*Nearfield Systems Inc. 1330 East 223rd St., Bldg. 524 Carson, CA 90745
**David Florida Laboratory, Canadian Space Agency
3701 Carling Avenue, Ottawa ON, Canada K2H 8S2

Abstract

This paper describes error analysis and measurement techniques that have been developed specifically for cylindrical near-field measurements. A combination of analysis and computer simulation is used to show the comparison between planar and cylindrical probe correction. Error estimates are derived for both the probe pattern and probe polarization terms. The planar analysis is also extended to estimate the effect of probe position errors. The cylindrical measurement geometry is very useful for evaluating the effect of room scattering from very wide angles since scans can cover 360 degrees in azimuth. Using a broad beam AUT and scanning over a large y-range provides almost full spherical coverage. Comparison with planar measurements with similar accuracy is presented.

Keywords: Analysis, Cylindrical near-field, errors, measurements.

1.0 Introduction

The NIST 18 term error model[1] was originally developed for planar near-field measurements, and it has been used frequently and successfully to estimate the uncertainties in specific measurements and to evaluate planar measurement facilities. Many of the tests and analyses that were developed for planar measurements can be applied without change to cylindrical measurements. For instance, probe gain, multiple reflections, receiver linearity, leakage and random errors can be evaluated on a cylindrical range using the same techniques that are used for planar measurements. Some of the analyses or tests do not transfer directly however, and these must be modified when applied to a cylindrical or spherical near-field range. This paper will report on the validation testing of a cylindrical near-field facility at the David Florida Laboratory and the new approaches that were developed for these tests. The cylindrical range with the VAST antenna mounted is shown in Figure 1. The VAST antenna is an offset reflector operating at X-Band. In this report special emphasis will be given to position errors, probe correction effects and room scattering tests. With the addition of analysis and measurements that were developed during this program, the NIST 18 term error model can be applied to any cylindrical near-field measurement.

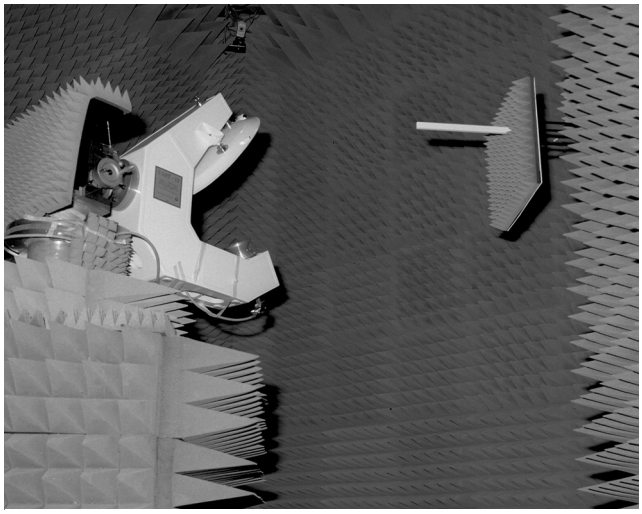

Figure 1 Test antenna and probe on DFL Cylindrical near-field range.

2.0 Probe Correction Equations for Planar and Cylindrical Near-Field Measurements

The probe correction in the cylindrical analysis is similar to the planar case and involves a pattern correction and a polarization correction. In the planar case, the probe correction equations for an X-polarized AUT reduce to,

$$t_A \cong \frac{D_A}{s_A'}, \quad (1a) \qquad t_E \cong \frac{D_E}{s_E''} - \frac{D_A}{s_A'}\rho_s'', \quad (1b) \quad (1)$$

In the above, a shorthand notation has been used for brevity, where $t_A \equiv t_A(\vec{K}) =$ Azimuth or horizontal component of AUT plane-wave spectrum. $t_E \equiv t_E(\vec{K}) =$ Elevation or vertical component of AUT plane-wave

spectrum. $s'_A \equiv s'_A(\vec{K}) =$ Azimuth or horizontal component of X-polarized probe's plane wave spectrum. $s''_E \equiv s''_E(\vec{K}) =$ Elevation or vertical component of X-Polarized probe's plane wave spectrum. $\mathrm{D_A} \equiv D_A(\vec{K}) =$ Fourier Transform of data measured with X-polarized probe. $\mathrm{D_E} \equiv D_E(\vec{K}) =$ Fourier Transform of data measured with Y-polarized probe. $\rho''_s \equiv \rho''_s(\vec{K}) =$ Probe's polarization ratio $= \frac{\mathrm{S''_A}}{\mathrm{S''_E}}$.

The only term in Equation (1a) and the first term in Equation (1b) correspond to the pattern correction and the second term in (1b) is the polarization correction. Since the far-field and the plane-wave spectra are nearly the same for both the AUT and the probe, the effect of errors in the probe pattern for planar measurements is straight forward. Pattern errors effect both the main and cross component results in the same direction and with the same magnitude as the probe errors. The polarization error is derived using Equations (1a) and (1b) giving (after some analysis)

$$\frac{p_t}{p_{t\varepsilon}} \cong 1 + p_t \rho''_s - p_t \rho''_{s\varepsilon} \quad \text{For x-Polarized AUT.} \quad (2)$$

$$\frac{p_{t\varepsilon}}{p_t} \cong 1 + \frac{1}{p_t \rho''_s} - \frac{1}{p_t \rho''_{s\varepsilon}} \quad \text{For y-polarized AUT.} \quad (3)$$

In Equations (2) and (3) $p_t =$ AUT polarization ratio $= \frac{t_A}{t_E}$. $p_{t\varepsilon} =$ AUT measured polarization ratio with error due to error in probe polarization denoted by $\rho''_{s\varepsilon}$.

The form of the probe correction equations for cylindrical near-field measurements is very similar to the planar case. But since there is an additional calculation after the probe correction to calculate the far-field, the final result of probe correction is much different. For example, for an X-polarized AUT the probe correction equations reduce to

$$T^1 \cong \frac{I'}{R'^1}, \quad (4a) \qquad T^2 \cong \frac{I''}{R''^2} + \frac{I'}{R'^1}\Re'' \quad (4b) \quad (4)$$

In Equation (4) $T^1 \equiv T^1_n(\gamma) =$ Horizontal component of AUT Cylindrical wave spectrum. $T^2 \equiv T^2_n(\gamma) =$ Vertical component of AUT Cylindrical wave spectrum. $\mathrm{R'^1} \equiv R'^1_n(\gamma) =$ Horizontal component, Cylindrical wave spectrum for X-polarized probe. $\mathrm{R''^2} \equiv R''^2_n(\gamma) =$ Vertical component Cylindrical wave spectrum for Y-polarized probe. $\mathrm{I'} \equiv \mathrm{I'_n}(\gamma) =$ Fourier Transform of data measured with X-polarized probe. $\mathrm{I''} \equiv \mathrm{I''_n}(\gamma) =$ Fourier Transform of data measured with Y-polarized probe. $\Re'' \equiv \Re''_n(\gamma) = \frac{R''^1_n(\gamma)}{R''^2_n(\gamma)} =$ Cylindrical polarization ratio for Y-polarized probe which measures the cross polarized data.

In the cylindrical case, neither the cylindrical wave spectra, T^1, T^2 nor the Fourier transforms, I', I'' are closely related to the far-field patterns. The calculation of the far-field pattern requires a Fourier series calculation in the A-direction where the contributions of the cylindrical coefficients are combined.

$$\vec{E}(r, A, E) = F(E) \sum_{n=-\infty}^{\infty} (-i)^n \left[T^1_n(\gamma)\hat{A} - iT^2_n(\gamma)\hat{E} \right] e^{inA}$$
$$\text{where } \gamma = k\,\mathbf{sin}(E) \quad \text{and} \quad \mathrm{F(E)} = \frac{-2ka_0\,\mathbf{cos}(E)\; e^{ikr}}{r} \quad (5)$$

Combining Equations (4a) and (5) for the main component pattern shows how the probe correction effects the far-field.

$$E_A(r, E, A) = F(E) \sum_{n=-\infty}^{\infty} (-i)^n \left[\frac{I'_n(\gamma)}{R'^1_n(\gamma)} \right] e^{inA} \quad (6)$$

Yajhian has shown[2] that the cylindrical probe correction coefficients, $R'^1_n(\gamma)$ are equal to the probe's far-field pattern. A particular probe coefficient is equal to the relative probe pattern at a given azimuth and elevation angle where γ defines the elevation angle, and n defines the azimuth angle. The AUT far-field pattern in a given direction is therefore affected by the probe pattern over a range of azimuth directions. The actual range depends on the measurement geometry and the ratio of the minimum cylinder radius to the measurement cylinder radius. For the measurements discussed here where the ratio of radii is 0.5, the probe pattern cuts between ± 30 degrees in Azimuth are used for the probe correction coefficients.

We can see the effect of the probe pattern correction by calculating far-field cuts with and without probe correction and comparing their difference with the probe pattern over the same angular region. Figure 2 shows the principal plane elevation cut for the AUT measured on the DFL range. The close comparison between the difference curve and the probe pattern shows that for the principle elevation cut the probe pattern correction is nearly equal to the probe pattern. However for the azimuth cut shown in Figure 3 the

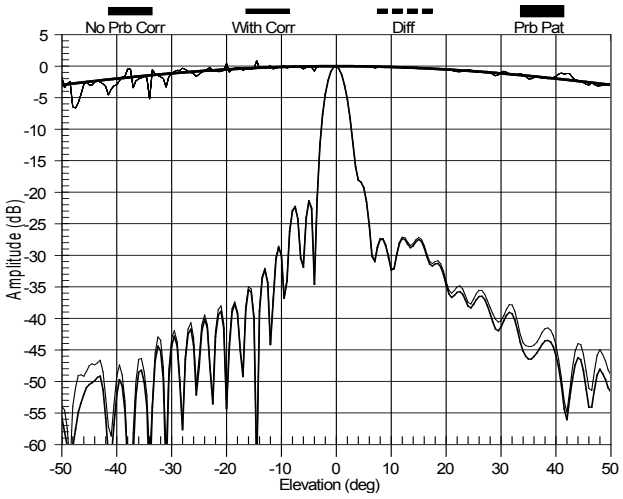

Figure 2 Far-field with and without probe correction and probe pattern curves, Elevation cut.

magnitude of the difference curve is significantly less than the probe pattern curve. Three conclusions can be made from Equation (6) and Figures 2 and 3 related to cylindrical probe pattern correction.

1- The probe correction for any given direction in the far-field is affected by the probe pattern over a range of azimuth values, not a single direction. This is true for both elevation and azimuth cuts as evidenced by the differences between the probe pattern and difference curves in Figures 2 and 3.

2- For each elevation angle and for azimuth angles near zero, the exponential term e^{inA}, in Equation (6) is approximately constant and the resulting probe pattern correction is approximately the probe pattern averaged over the azimuth angles. The difference curve and the probe pattern agree in Figure 2 because the change in the average at different elevation angles is the same as the change in the elevation cut.

3- For azimuth angles beyond the main beam, the exponential term will alternate between plus and minus, real and imaginary, and the resulting probe pattern correction will be small.

4- For any direction in the far-field, the change in the AUT far-field due to an error or uncertainty in the probe's pattern at a single direction in its pattern is given by,

$$\Delta E_A(r,E,A) = F(E)\frac{I'_M(\gamma)}{R'^1_M(\gamma)}\left[\frac{\Delta R'^1_M(\gamma)}{R'^1_M(\gamma)}\right]e^{iMA} \qquad (7)$$

where the index M defines the specific azimuth direction of the probe error. A combination of analysis and computer simulation has shown that an amplitude error in the probe pattern in a single direction produces an approximately isotropic far-field error pattern as shown in Figure 4. For an amplitude error of ε dB in the probe pattern, the Error to Signal level of this error pattern is

$$ERR/SIG \le 20 * \mathbf{log}(10^{\varepsilon/20} - 1) - G_{AUT} \qquad (8)$$

where G_{AUT} is the gain of the AUT in dB. For the simulation in Figure 4, the probe error was 1 dB and the AUT gain was 30 dB. Equation (8) predicts an error level of approximately -48 dB that is consistent with the results shown in Figure 4. This error would occur in all far-field directions. By comparison, the same error in a planar measurement would produce an error to signal level of -18 dB at only one direction in the far-field.

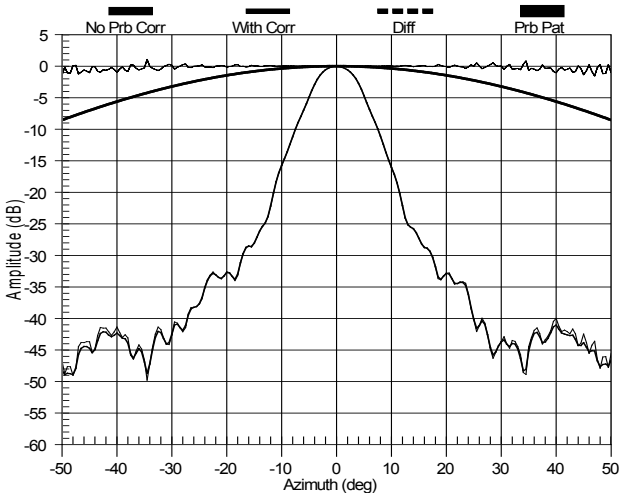

Figure 3 Far-field with and without probe correction and probe pattern curves, Azimuth cut.

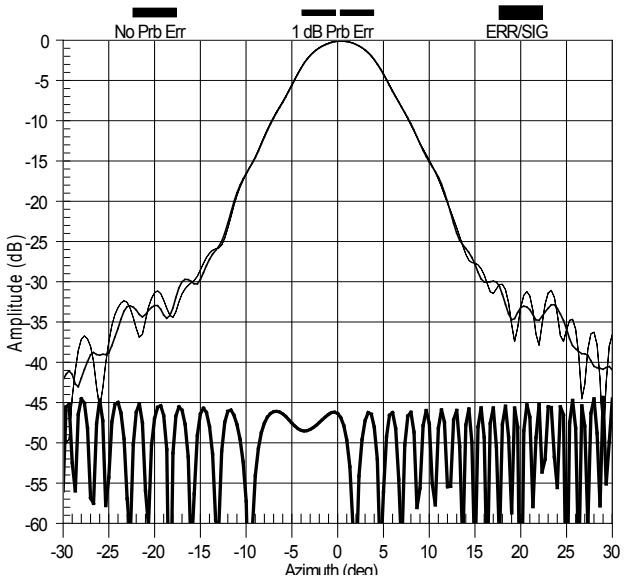

Figure 4 Results of simulating an error in the probe's pattern for cylindrical near-field.

3.0 Probe Polarization Error Estimates for Cylindrical Near-Field Measurements

The polarization probe correction effect on the far-field cross component comes from combining Equations (4b) and (5).

$$E_E(r,E,A) = F(E)\sum_{n=-\infty}^{\infty}(-i)^{n+1}\left[\frac{I_n''(\gamma)}{R_n''^2(\gamma)} + \frac{I_n'(\gamma)}{R_n'^1(\gamma)}\Re_n''(\gamma)\right]e^{inA} \tag{9}$$

The polarization correction is due to the second term in (9) and is due to the cross-polarization of the probe that measures the cross component near-field data as represented by the factor $\Re_n''(\gamma)$ in (9). The error is due to the uncertainty in our knowledge of the probe's polarization ratio, $\Re_n''(\gamma)$. For a typical probe, the second term in (9) is small as shown in Figure 5 and can be estimated as approximately equal to the product of the main component pattern of the AUT times the cross component pattern of the probe. These two patterns along with the resulting polarization correction term are shown in Figure 5 and

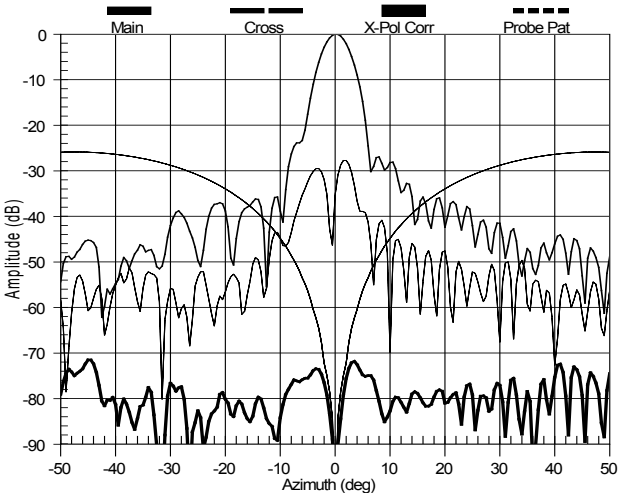

Figure 5 Example of relative magnitude of terms in polarization probe correction for 45 degree cut.

labeled respectively Main, Probe Pat, and X-Pol Corr. The pattern cuts along the 45 degree diagonal are used for this example since the cross polarization correction is larger in this region. Analysis and comparison to planar results show that Equations (2) and (3) give good estimates of the error in cylindrical measurements with the following modifications. 1- The cross polarization of the AUT at a single direction is affected by the probe's polarization ratio over a small region of azimuth angles. For the example in Figure 5 the region appears to be approximately 5-10 degrees. 2- The average error over the region, not the error in one direction should be used in Equation (2) or (3) to estimate the resulting far-field error. For example at +2 degrees in Figure 5, the polarization ratio of the AUT is approximately +24 dB and the polarization ratio for the probe is approximately -70 dB. From Equation (2) an error of 5 dB in the probe polarization in the region of 2 degrees would result in an error of only 0.03 dB in the AUT cross component pattern. In the sidelobe region where the probe polarization is not as good, the AUT polarization also is worse and for example at 30 degrees, the error due to a 5 dB error in the probe is still only 0.2 dB.

4.0 Y-Position Errors

For Y errors, the theoretical treatment for X-Y errors in planar measurements can be used. For the case where the main beam is approximately normal to the Y-axis, the errors in gain and sidelobe are,

$$\Delta G_{dB}(E,A) \le \frac{8.7\,\Delta_y\,(RMS)}{\eta L_y}\,g(E,A)\,[Main\ Beam]$$
$$\Delta P_{dB}(E,A) \le \frac{4.3\,\Delta_y\,(E,A)}{L}\,g(E,A)\,[Sidelobes] \tag{10}$$

where G is the antenna gain, P the relative pattern L the antenna major dimension, η the aperture efficiency, and Δ_y the y position error. g(E,A) is the reciprocal of the sidelobe level in voltage not dB, for instance, for a –40 dB sidelobe, g(E,A) is 100.

5.0 Probe radius and azimuth position errors

The effect of errors in the radius is similar to the z-position errors in planar measurements since it mainly produces a phase error as a function of y and azimuth. For a fan beam AUT where the near-field phase is essentially constant on a cylinder, the equation for radius errors is identical to the z-error equation for planar. But for a pencil beam antenna, the amount of phase change for a given radius error varies with azimuth angle. As a result we will use the planar equations for the case of a beam steered to 45 degrees from the z-axis which will approximate the average phase error in the cylindrical case. The two equations for the main beam and sidelobe region are,

$$\Delta G_{dB}(E,A) \le \frac{22}{\sqrt{\eta}}\left(\frac{\delta_r(rms)}{\lambda}\right)^2 g(E,A)[Main\ Beam] \tag{11}$$

$$\Delta P_{dB}(E,A) \le \frac{10\,\delta_r(\theta,\phi)}{\lambda}\,g(E,A)[Sidelobes] \tag{12}$$

The effect of azimuth position errors can also be determined by using a modified version of the z-error equations. The modification uses the z-position error induced by an azimuth position error. The z-position of the probe as it moves on the measurement cylinder and the z-error that results are respectively,

$$z = r(\cos(A) - 1), \quad \delta_z(AZ) = r \sin(A)\ \delta_A \qquad (13)$$

The z-position errors that produce the major effect are those that occur within the collimated region of the near-field which is essentially within the aperture region of the AUT. For an antenna with an aperture width of L_x in the x-direction, the collimated region on the measurement cylinder is bounded approximately by the azimuth angles,

$$A_c = \pm \arcsin\left(\frac{L_x}{2r}\right) \qquad (14)$$

The z-error will therefore vary between zero when A=0 and a maximum of

$$\delta_z(A) = \frac{\pi L_x \delta_A}{360} \quad \text{for } \delta_A \text{ in degrees} \qquad (15)$$

The average z-error equal to one half of Equation (15) is used in Equations 11 and 12 with $\delta_r = \delta_z$ to determine the effect of azimuth position errors.

In addition to the estimates using the planar analysis, measurement tests were also performed where a specific position error was induced by mis-aligning the azimuth rotator. The base of the tower was tilted to induce a known angular tilt between the y-axis and the azimuth axis of rotation. This is a typical type of position error that might be encountered in cylindrical measurements. The tower was rotated about its x-axis by 0.1 degrees and a measurement was performed. Comparison of the far-field patterns with and without the alignment error gives a direct measure of the effect of this specific kind of error. The rotation of the tower produces a maximum radius error of 0.044 inches and an RMS error of 0.03 inches. Equation (11) predicts a gain error of 0.05 dB and the observed gain change was 0.052 dB.

6.0 Room Scattering Measurements

Room scattering errors are the combined multipath scattering effects of everything in the near-field range other than the probe. This includes the scanner, floor, ceiling and other fixed objects in the room. This quantity is usually identified by changing the AUT Z position while keeping the probe-to-AUT separation distance constant.

Measurements are made at each Z-position, the far-fields are calculated, and the patterns are subtracted. If the alignment is not changed, and all other errors should remain constant, any change should be due to changes in the room scattering. In the measurements taken in the the DFL near-field range, room scattering measurements were performed using the VAST antenna shown in Figure 1 and also using a standard gain horn. In both cases, measurements were performed with the probe and AUT at 0, 4 and 9 inches. The horn gave more complete evaluation of the scattering since its broad pattern illuminated more of the room. The azimuth span was over 360 degrees for the room scattering tests and the y-span was also increased to increase the elevation coverage.

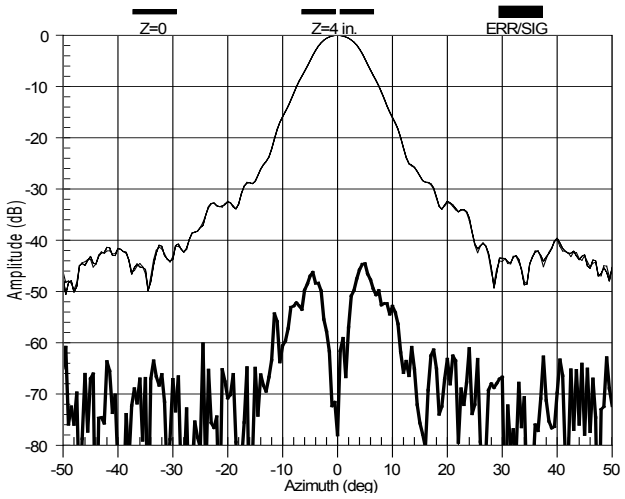

Figure 6 Results of room scattering showing peaks near boresight due to alignment changes.

The pattern subtraction is very sensitive to small changes in the magnitude and position of the beam peak. Since we are trying to measure scattering levels of -40 to -60 dB below the peak amplitude, differences in peak amplitude of only a few hundredths of a dB and beam alignment changes of hundredths of a degree effect the results significantly. This is illustrated in Figure 6 which shows the results of a scattering test on the Vast antenna. The curve identified as ERR/SIG is derived from the difference in the far-field patterns measured at the two Z-distances. It is a measure of the room scattering relative to the antenna main beam signal. The two peaks near boresight are not actually due to room scattering but are due to small changes in the antenna angular alignment when it is moved in Z. If the pattern taken at 4 inches is shifted in azimuth by 0.030 degrees and in elevation by 0.01 degrees the peaks disappear and the full curve is below -60 dB. It is important to look closely at the beam peaks and to adjust for small alignment changes before calculating the room scattering so that such effects are not misinterpreted as room scattering.

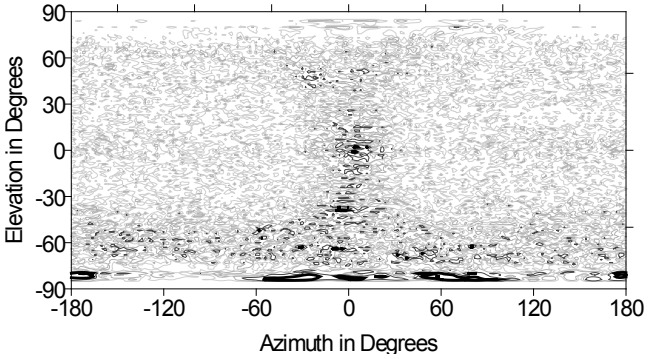

Figure 7 Contour plot of room scattering results on the DFL cylindrical range from standard gain horn measurements

In addition to single cuts similar to Figure 6, contour and surface plots that covered the full measurement sphere were also generated from the standard gain horn data. These give a much more complete evaluation of the room scattering from the complete range. One result is shown in Figure7 as a contour plot. The darkest contours near -90 degrees in elevation and near 0 degrees in azimuth are at -45 dB. The adjacent medium dark contours are at -50 dB,

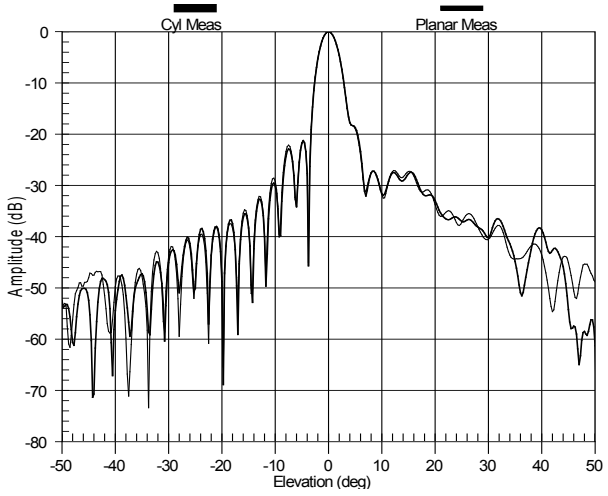

Figure 8 Comparison of main component far-field pattern results from planar and cylindrical near-field measurements.

and the gray contours are at -55 dB. The majority of the contours in the regions above -30 degrees in elevation and beyond the elevation centerline are at -60 dB. The main features that represent actual room scattering are those between -60 and -90 degrees in elevation. These features were in all of the results from the horn measurements and are probably due to lights and other scattering objects that were in the ceiling above the measurement range. These tests confirm that there are no scattering objects other than the ceiling within the measurement facility that adversely effect the patterns above the -55 dB level.

7.0 Comparison With Planar Results

The VAST antenna was used previously for measurements at an NSI planar near-field facility and the data from those measurements was available for comparison. Figures 8 and 9 show the comparison of main and cross component patterns obtained on the cylindrical and planar ranges. The agreement between the measurements was consistent with the estimates of uncertainty for the two ranges.

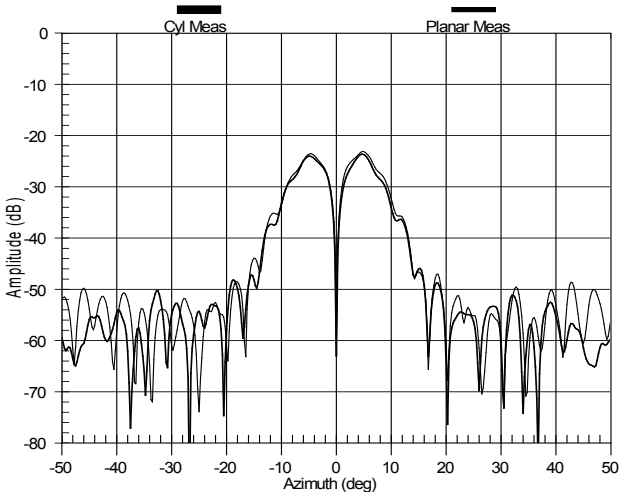

Figure 9 Comparison of cross component far-field pattern results from planar and cylindrical near-field measurements.

8.0 Conclusions

Mathematical analysis and measurement techniques have been developed that extend the NIST 18 term error analysis to cylindrical measurements. These new developments were for probe pattern and polarization errors and cylindrical position errors. In addition results of room scattering tests have demonstrated the unique ability of the cylindrical measurements to evaluate all of the measurement facility.

---

[1] Newell, A. C., "Error analysis techniques for planar near-field measurements," *IEEE Transactions on Antennas and Propagation, Vol.* AP-36, pp. 755-768, June 1988.

[2] Yaghjian, A.D., "Antenna Measurements on a CylindricalSurface: A Source Scattering-Matrix Approach", National Bureau of Standards Technical Note 696, 1977, 34 p., Boulder, CO.